Feasibility Study of a Hybrid Wind Turbine System - Integration with Compressed Air Energy Storage

Hao Sun[1,2,#], Xing Luo[1,#], Jihong Wang[1,*]

[1] School of Engineering, University of Warwick, Coventry CV4 7AL, UK

[2]School of Electronic, Electrical and Computer Engineering, University of Birmingham Birmingham B15 2TT, UK

[#] The two authors have made equal contributions to this paper.

* Correspondence Author: Email: jihong.wang@warwick.ac.uk, Tel: 0044-247-6523780.

***Abstract*—**Wind has been recognized as one of major realistic clean energy sources for power generation to meet the continuously increased energy demand and to achieve the carbon emission reduction targets. However, the utilisation of wind energy encounters an inevitable challenge resulting from the nature of wind intermittency. To address this, the paper presents the recent research work at Warwick on the feasibility study of a new hybrid system by integrating a wind turbine with compressed air energy storage. A mechanical transmission mechanism is designed and implemented for power integration within the hybrid system. A scroll expander is adopted to serve as an "air-machinery energy converter", which can transmit additional driving power generalized form the stored compressed air to the turbine shaft for smoothing the wind power fluctuation. A mathematical model for the complete hybrid process is developed and the control strategy is investigated for corresponding cooperative operations. A prototype test rig for implementing the proposed mechanism is built for proof of the concept. From the simulated and experimental studies, the energy conversion efficiency analysis is conducted while the system experiences different operation conditions and modes. It is proved that the proposed hybrid wind turbine system structure is feasible technically.

***Index*—** wind turbines, compressed air energy storage, hybrid systems, mathematical modelling, control strategy.

1. Introduction

In recent years, wind power generation has shown a robust growth trend worldwide. The global cumulatively installed generation capacity of wind power reached 318,137 MW at the end of 2013, which has increased by more than 163% compared to 120,624 MW in 2008 [1]. Such rapid development is mainly driven by the continuous increase in electricity demand and the need for reducing greenhouse gas emissions. However, the nature of fluctuation and intermittence of wind makes it very difficult to deliver power output from wind energy with an instant match to the electricity demand. This nature also brings the negative impact

onto the wind turbine system operation efficiency, life expectance and mechanical structures [2]. Thus, new technologies and approaches have been actively researched to alleviate the problems caused by wind fluctuation and intermittence, such as wind turbine pitch angle control, power electronics development for wind power and flexible back-up power generation [3, 4, 5]. One of the promising solutions is to introduce an element of stored energy as an alternative energy supply for use when the ambient wind power is insufficient. Various Energy Storage (ES) technologies can provide the service of compensators to work with different types of wind power generation systems, for example, hydroelectric pumped storage, Compressed Air Energy Storage (CAES), flow batteries and flywheels [6, 7]. Among the available ES technologies, CAES can be considered as one of the relatively mature and affordable options [6, 8, 10].

CAES technology refers to storing energy in the form of high pressure compressed air during the periods of low electrical energy demand and then releasing the stored energy during the high demand periods. CAES facilities exist in multiple scales, with long storage duration, moderate response time and good part-load performance [6, 7, 9]. So far, there are a few successful industrial implementations of large-scale CAES plants serving wind power generation. For instance, after the world first commercialized Huntorf CAES plant started operation, its mandate was updated to include the buffering against the intermittence of wind energy production in Northern Germany [9]. Also, the developing advanced adiabatic CAES demonstration project – ADELE by RWE Power and others aims to store large amounts of electrical energy through CAES and thermal storage concepts; the ADELE plans to operate with wind farms, with a storage capacity of 360 MWh without CO_2 emissions [11, 12].

In addition to the large-scale CAES facility integrated with the wind power generation, the work presented in the paper is to explore the potential of using smaller scale CAES in the wind power application. Inspirited by the parallel drive train in Hybrid Electrical Vehicles (HEVs) ([13]), this paper presents a novel direct electromechanical integration of a wind turbine system and a CAES mechanism at a few kWs scale. The objective is to develop a system with simple structure, efficient, low maintenance, clean and sustainable. The proposed design is illustrated in Fig. 1. It consists of three main sections:

(1) Wind turbine subsystem: this subsystem simulates a real scenario of horizontal wind turbines' operation. It includes a module of wind power extracted by blades, a mechanical drive train, a Permanent Magnet Synchronous Generator (PMSG) and its load(s) to be driven. The generated electricity can be directly used to end-users or fed back to grids via electric power converters and inverters.

(2) CAES subsystem: it is composed of a scroll expander and a compressed air storage tank. This relatively new type of expander has a smart mechanical structure leading to a higher energy conversion ability compared to most other pneumatic drives. Due to the capacity of typical scroll expanders, the proposed structure is more suitable for small-scale wind turbine systems. The compressed air stored in the tank can be obtained from the operation of compressors on site or local suppliers. From Fig. 1, through a mechanical transmission mechanism, an additional driving power by the CAES subsystem can provide a direct compensation to the wind turbine.

(3) Controller: for managing the whole hybrid system's operation, an appropriate control strategy is particularly important for supporting the system multi-mode operations and ensuring the dynamic balance of driving power and electric load demand.

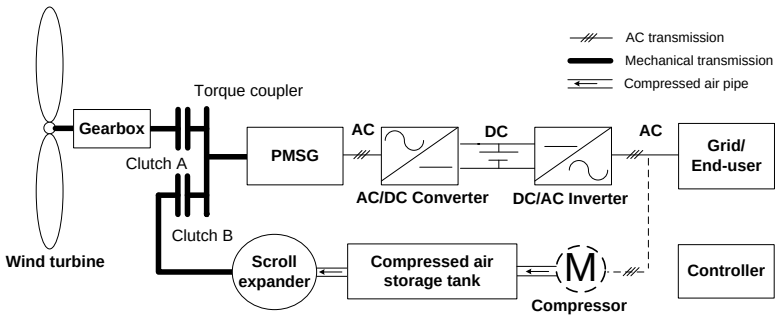

Fig.1 Small-scale hybrid wind turbine with CAES

Study of hybridization of wind generation with CAES was reported in various literatures, for example, [14-17]. The common feature of the previously reported hybridization systems is that CAES is treated as an independent energy storage unit and is engaged with wind power generation through management of electricity network connection. The hybrid system proposed in this paper is mainly new and different because the CAES is directly connected to the turbine shaft through a mechanical transmission mechanism. In this way, with a proper control strategy, the compressed air energy will be released via the direct mechanical connection to contribute to wind turbine power generation. Thus the system does not require a separate generator and extra electricity conversion device(s) which will reduce the whole system cost. In addition, the extra torque input from the air expander could reduce the turbine shaft stress for prolonging the turbine life time.

The paper starts from description of the hybrid system, development of its mathematical model, and presentation of a suitable multi-mode control strategy. Then a hybrid wind turbine test rig is reported, which is installed in the authors' research laboratory. Finally the whole system energy conversion efficiency analysis is given.

2. Mathematical model of the hybrid wind turbine system

In this subsection, the mathematical models for a typical wind turbine, a Permanent Magnet Synchronous Generator (PMSG), a scroll expander and a novel mechanical power transmission system are presented, and then the whole system control strategy is described. In the modelling study, it is assumed that the air supply of the scroll expander, i.e., the compressed air from the storage tank, is sufficiently pre-compressed air with constant temperature. Thus the scroll expander air supply can be regarded as a controllable compressed air source.

2.1 Mathematical model for wind turbines

A typical horizontal axis wind turbine is chosen in the hybrid system for modelling study. Its mechanical power output *P* which can be produced by the turbine at the steady state is given by:

$$P = \frac{1}{2}\rho_a \pi r_T^2 v_w^3 C_p \tag{1}$$

where ρ_a is the air density; r_T is the blade radius; v_w is the wind speed; C_p represents the turbine efficiency, revealing the capability of turbine for obtaining energy from the wind. This coefficient depends on the tip speed ratio and the blade angle. Because the calculation of C_p requires the knowledge of aerodynamics and the computations are quite complicated, some numerical approximations to (1) were developed and studied [18, 19]. In this hybrid system modelling, the following function is adopted to approximate the calculation presented in (1) [18, 20],

$$C_p(\lambda,\theta) = 0.22\left[\frac{116(\lambda\theta^3+\lambda+0.08\theta^4+0.08\theta)}{\theta^3-0.035\lambda-0.0028\theta+1} - 0.4\theta - 5\right]e^{-\frac{12.5(\lambda\theta^3+\lambda+0.08\theta^4+0.08\theta)}{\theta^3-0.035\lambda-0.0028\theta+1}} \tag{2}$$

where θ represents the pitch angle, λ stand for the tip speed ratio, $\lambda = \omega_T \cdot r_T / v_w$, ω_T is the turbine speed. Eq. (2) lead to $C_p(\lambda, \theta)$ versus λ characteristics for various values of θ as depicted in Fig. 2. It can be seen that the power coefficient C_p varies with different values of the pitch angle θ (for instance, $\theta = 0^o, 5^o, 10^o$ and 15^o as shown in Fig. 2), and the best efficiency is obtained at $\theta = 0^o$ in most cases [21]. From the above, the mechanical driving power extracted from the wind can be calculated by Eq. (1) and (2).

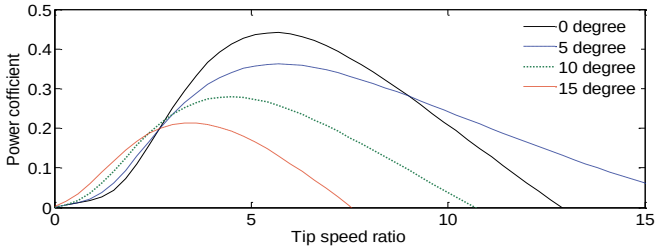

Fig. 2 Power coefficients as a function of tip speed ratio and pitch angle

The drive train of a wind turbine system normally consists of a blade pitching mechanism with a spinner, a hub with blades, a rotor shaft, a gearbox with brake and sometimes a generator. The generator impact on the whole hybrid system will be considered in the mechanical power transmission modelling in the later subsection. Thus to the proposed system, for describing the dynamic behaviours of the pure wind turbine, a simplified mathematical model is considered,

$$\frac{d}{dt}\omega_T = \frac{1}{J_T}(\tau_T - \tau_L - B\omega_T) \tag{3}$$

where ω_T and J_T are the rotation speed and the inertia of turbine blades respectively, τ_T and τ_L stand for the torques of wind turbine and low-speed shaft individually, B is the damping coefficient of the driven train system. The low-speed shaft is connected and driven by the turbine rotor.

2.2 Mathematical model for scroll expanders

The scroll expander, also known as the scroll type air motor, is a relatively new member to pneumatic drives. Such type of expander is famous with its high efficiency and its unique smart mathematical structure [22, 23], which is the key component in the proposed small-scale hybrid wind turbine system. Fig. 3 shows the mechanical structure of a typical scroll expander. It can be seen that, inside the expander shell, there are two intermeshed identical scrolls, namely the moving scroll and the fixed scroll. Each scroll is fitted with a back plate. Both two scrolls are circular involutes. One scroll is mirrored with respect to the other. The crank shaft of the scroll expander connects to the back plate of the moving scroll through a cam and bearing mechanism.

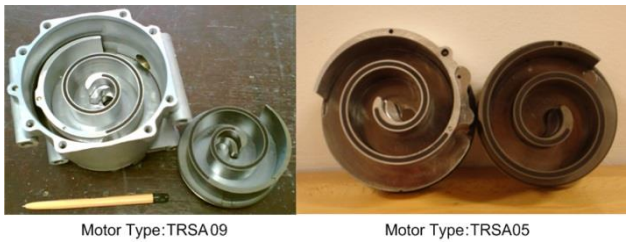

Fig. 3 Illustration of the scroll expander structure (manufactured by Sanden)

A scroll expander with three wraps in motion and its moving scroll orbit trajectory is illustrated in Fig. 4. The black scroll stands for the moving scroll and the grey one represents the fixed scroll. The moving scroll travels along the orbit anticlockwise when the compressed air comes into the scroll mechanism. During the expander operation, these two scrolls always keep contacting at some points. This forms three different types of air chambers inside the expander shell: a central chamber, even number of sealed crescent chambers and an exhaust chamber. The early work by the authors has proven that the scroll expander has more energy efficient

performance compared to conventional pneumatic drives with similar scales (up to several kW level), such as reciprocating cylinders, vane type air motors, etc. [24].

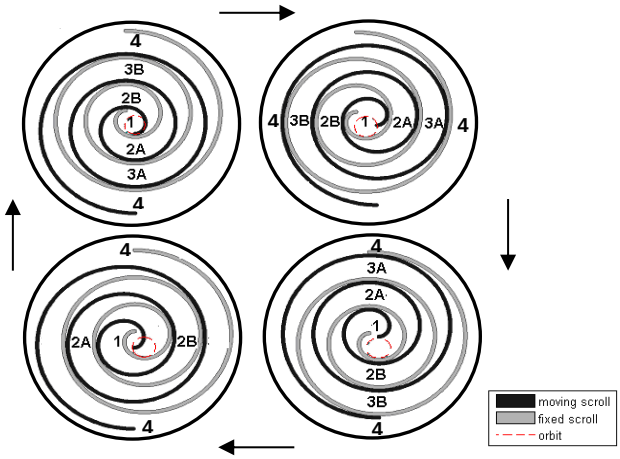

Fig. 4 Schematic diagram of a scroll expander in motion

With the following assumptions: 1) no air leakage, 2) the scroll expander using ideal air and 3) it working at a constant temperature environment, a simplified mathematical model for scroll expanders can be derived [22, 24, 25]. The geometric model for scroll expanders can be derived from the fundamental curve of a spiral. The equations for the moving scroll can be described by,

$$x_{\mathbf{A}}(\varphi_s,\alpha_s)=x_0+(\rho_0+\kappa_s\varphi_s)\sin\varphi_s+\kappa_s\cos\varphi_s-\kappa_s+r_s\sin\alpha_s \quad (4)$$

$$y_{\mathbf{A}}(\varphi_s,\alpha_s)=y_0-(\rho_0+\kappa_s\varphi_s)\cos\varphi_s+\kappa_s\sin\varphi_s+\rho_0-r_s\cos\alpha_s \quad (5)$$

where $(x_{0,}\ y_0)$ is the initial position and ρ_0 is the initial curvature radius for the moving scroll curve, κ_s is the slope of the curvature radius, r_s refers to the orbit radius of the moving scroll, α_s stands for the scroll expander orbit angle, φ_s is the tangential angle to the moving scroll. The fixed scroll is generated by the curve which envelops the family of the moving scroll curves when the moving scroll wobbles along with its orbit [22]. The equations for the fixed scroll can be,

$$x_{\mathbf{B}}(\phi_s)=x_1-(\rho_0+\kappa_s\phi_s)\sin\phi_s-\kappa_s\cos\phi_s+\kappa_s \quad (6)$$

$$y_{\mathbf{B}}(\phi_s)=y_1+(\rho_0+\kappa_s\phi_s)\cos\phi_s-\kappa_s\sin\phi_s-\rho_0 \quad (7)$$

where ϕ_s is the tangential angle to the fixed scroll, $(x_{1,}\ y_1)$ is the initial position for the fixed scroll curve, and the moving scroll contacts the fixed scroll at the points, thus $\varphi_s=\phi_s+j\pi$, j is an arbitrary integer [22].

Applying Green's Theorem, the equations for describing the volume variations of the scroll expander chambers can be derived [25]. The control volume of the central chamber is,

$$V_c(\alpha_s) = z[(x_0\kappa_s\pi - \kappa_s{}^2\pi - x_0 r_s + r_s\kappa_s)\cos\alpha_s + \kappa_s{}^2\pi\alpha_s{}^2 + (r_s\rho_0\kappa_s\pi - r_s\rho_0 - y_0 r_s + y_0\kappa_s\pi)\sin\alpha_s - r_s\kappa_s + \frac{1}{3}\kappa_s{}^2\pi^3 + (r_s\pi\kappa_s + 2\kappa_s\rho_0\pi)\alpha_s - \frac{1}{2}r_s\pi^2\kappa_s + \rho_0 r_s\pi + \frac{1}{2}r_s{}^2\pi + \rho_0^2\pi] \quad (8)$$

where $V_c(\alpha_s)$ is the volume of scroll expander central chamber, z is the depth of the moving and fixed scrolls. The control volume of the i^{th} (i=1, 2, 3…) pair of sealed crescent chambers is:

$$V_s(\alpha_s, i) = z[\pi r_s{}^2 + 2\pi r_s(\rho_0 + \kappa_s(\alpha_s + \pi + 2(i-1)\pi))] \quad (9)$$

where $V_s(\alpha_s, i)$ is the volume of scroll expander sealed crescent chamber volume. The control volume of the exhaust chamber can be described by,

$$V_e(\alpha_s) = V_{total} - V_c(\alpha_s) - \sum V_s(\alpha_s, i) \quad (10)$$

where $V_e(\alpha_s)$ is the volume of scroll expander exhaust chamber volume, V_{total} represents the total control volume of the scroll expander.

From the fundamental of thermodynamics and the theory of orifice, the air pressure of the different scroll expander chambers can be calculated [22, 24, 25]. To the air pressure variation of the central chamber ($\dot{p}_c$),

$$\dot{p}_c = -\frac{\dot{V}_c}{V_c}p_c\omega_s\gamma + \frac{1}{V_c}\gamma R C_d C_0 C_k A_i p_s f(p_c / p_s)\sqrt{T_s} \quad (11)$$

To the air pressure variation of the first pair of sealed crescent chambers ($\dot{p}_{s1}$),

$$\dot{p}_{s1} = -\frac{\dot{V}_s(\alpha_s,1)}{V_s(\alpha_s,1)}p_{s1}\omega_s\gamma \quad (12)$$

To the air pressure variation of the second pair of sealed crescent chambers ($\dot{p}_{s2}$),

$$\dot{p}_{s2} = -\frac{\dot{V}_s(\alpha_s,2)}{V_s(\alpha_s,2)}p_{s2}\omega_s\gamma \qquad \alpha_s \in [0,\ \pi] \quad (13)$$

To the air pressure variation of the exhaust chamber ($\dot{p}_e$),

$$\dot{p}_e = -\frac{\dot{V}_e}{V_e}p_{s2}\omega_s\gamma + \frac{1}{V_e}\gamma R c_d c_0 c_k A_o p_e f(p_{atm} / p_e)\sqrt{T_s} \quad (14)$$

The driving torque generated by a scroll expander is the sum of torques on all driving segments on the two scrolls, and it can be derived as [22, 24, 25],

$$\tau_s = \begin{cases} zr[(2\rho_0 + 2\kappa_s\alpha_s + \kappa_s\pi)(p_c - p_{s1}) + (2\rho_0 + 2\kappa_s\alpha_s + 5\kappa_s\pi)(p_{s1} - p_{s2}) + (2\rho_0 + 2\kappa_s\alpha_s + 9\kappa_s\pi)(p_{s2} - p_e)] & \alpha_s \in [0, \pi] \\ zr[(2\rho_0 + 2\kappa_s\alpha_s + \kappa_s\pi)(p_c - p_{s1}) + (2\rho_0 + 2\kappa_s\alpha_s + 5\kappa_s\pi)(p_{s1} - p_e)] & \alpha_s \in (\pi,\ 2\pi] \end{cases} \quad (15)$$

where p_s is the supply pressure, p_{atm} is the pressure of atmosphere, T_s is the supply temperature, R is the gas constant, $c_0 = 0.04$, $c_d = 0.8$, $c_k = 3.864$, γ = 1.4 is the ratio of specific heat, A_i, A_o are the effective area of expander inlet and outlet respectively, r_s is the radius of the orbit, ω_s is the rotation speed of scroll expander shaft, $f()$ is a function of the ratio between the downstream and upstream pressures at the orifice [24, 25]. In the modelling, it should be noticed that, when the orbit angle $\alpha_s \in (\pi, 2\pi]$, the second pair of crescent chambers is not sealed anymore in each period (refer to Fig. 4).

2.3 Mathematical model for permanent magnet synchronous generators

A Permanent Magnet Synchronous Generator (PMSG) has been chosen as the driven machine of the wind turbine; a resistive load is directly connected to the PMSG electricity output for simplicity of analysis. The mathematical model is described by Eq. (16-22), which has been studied in [26-28]:

$$\frac{d\omega_G}{dt} = \frac{1}{J_G}(\tau_G - \tau_e - F_G\omega_G) \tag{16}$$

$$\frac{d\theta_G}{dt} = \omega_G \tag{17}$$

$$\frac{di_d}{dt} = \frac{1}{L_d}v_d - \frac{R_G}{L_d}i_d + \frac{L_q}{L_d}p_G\omega_G i_q \tag{18}$$

$$\frac{di_q}{dt} = \frac{1}{L_q}v_q - \frac{R_G}{L_q}i_q - \frac{L_d}{L_q}p_G\omega_G i_d - \frac{\varepsilon p_G\omega_G}{L_q} \tag{19}$$

$$\tau_e = 1.5p_G[\varepsilon\, i_q + (L_d - L_q)i_d i_q] \tag{20}$$

$$v_q = \frac{1}{3}[\sin(p_G\theta_G)\cdot(2v_{ab} + v_{bc}) + \sqrt{3}v_{bc}\cos(p_G\theta_G)] \tag{21}$$

$$v_d = \frac{1}{3}[\cos(p_G\theta_G)\cdot(-2v_{ab} - v_{bc}) - \sqrt{3}v_{bc}\sin(p_G\theta_G)] \tag{22}$$

where the subscripts a,b,c,d,q mean the a,b,c,d,q axis respectively, θ_G and ω_G are the PMSG rotor angular position and speed respectively, τ_G and τ_e stand for the PMSG driving and electromagnetic torques, J_G is the inertia of the PMSG, R_G is the resistance of the stator windings, L_q, L_d are the resulted q and d axis inductances respectively, p_G is the number of PMSG pole pairs, $\boldsymbol{i}$ and v are the current and voltage in the different axes, ε is the flux amplitude induced by the permanent magnets of the rotor, F_G is combined viscous friction of the generator rotor. The Park's transformation is employed for transforming $\vec{\mathbf{X}}_{abc}$ (3-phase coordinates) to $\vec{\mathbf{X}}_{dq}$ (DQ rotating coordinates) [26, 28].

2.4 Mathematical model for the mechanical power transmission

The designed power transmission system mainly includes two electromagnetic clutches and a belt speed transmission to ensure coaxial running, as shown in Fig. 5. The functions of two clutches are described below: (1) Clutch A is engaged in almost all cases. Unless the wind speed is extremely low - under the cut-in wind speed, Clutch A will be disengaged and then the PMSG will be exclusively driven by the scroll expander. For the simplicity of modelling, the extreme low wind speed (Clutch A disengagement) situation is not considered. (2) Clutch B is placed to the hybrid system for conditional switching on/off the small-scale CAES subsystem. When the wind turbine cannot generate sufficient electricity to match the electric load demand, the compressed air in the storage tank will be released into the scroll expander via a pneumatic valve and/or regulator's control; then the scroll expander will start rotating and Clutch B will be engaged at the moment of the expander rotor speed comparably to the wind turbine shaft speed after the belt transmission. Also, Belt plate A and B of the belt transmission have different diameters to play the function as a gearbox (refer to Fig. 5). Thus the small-scale CAES subsystem and the wind turbine can be integrated rigidly.

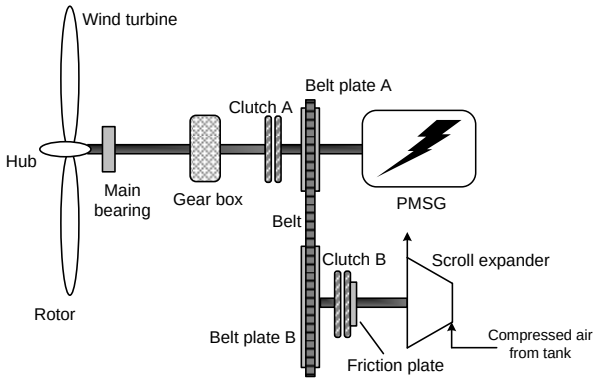

Fig. 5 Structure of the mechanical power transmission in the hybrid wind turbine system

According to the above description, the main working states with their mathematical expressions of the mechanical power transmission can be derived:

Case I. Clutch A engaged and Clutch B disengaged: the two disks of Clutch B is fully separated (refer to Fig. 5). Considering friction and different payloads, applying Newton's second law of angular motion, to the shaft of scroll expander, we have,

$$\tau_s - M_f \omega_s = (J_s + J_f)\dot{\omega}_s \tag{23}$$

where J_s is the scroll expander inertia, J_f is the friction plate inertia, τ_s is the scroll expander driving torque; M_f is the combined viscous friction coefficient; $\dot{\omega}_s$ represents the scroll expander angular acceleration.

To the main shaft of the wind turbine system, both the active plate and the passive plate of the belt transmission can be considered as an extra inertia load, thus the total equivalent inertia can be,

$$J_{total} = J_{pass} + \varsigma^2 J_{act} \tag{24}$$

where J_{pass} and J_{act} are the inertias of the passive and active plate respectively, ς is the speed ratio of the belt.

Case II. Both Clutch A and Clutch B engaged: Once Clutch B is engaged by coupling its two disks, the following equations can be derived:

$$\begin{cases} \tau_s - M_f \omega_s - \tau_{act} = (J_s + J_f + J_{act})\dot{\omega}_s \\ \tau_{pass} = \tau_{act}\eta\varsigma \\ \tau_H + \tau_{pass} - \tau_e - F_G\omega_G = \dot{\omega}_G(J_G + J_{pass}) \\ \omega_s = \omega_G\varsigma \end{cases} \tag{25}$$

where τ_H is the torque of wind turbine high-speed shaft. The high-speed shaft is linked to the output of gearbox (refer to Fig. 5). η is the transmission efficiency of the belt.

2.6 Overall state space model of the hybrid system

With all the subsystem models presented above, the overall state space model for the hybrid system is presented below. The system state variables are chosen: x_1: PMSG rotor angle, x_2: PMSG angle velocity, x_3: current in d axis for PMSG, x_4: current in q axis for PMSG, x_5: pressure in the expander central chamber, x_6: pressure in the expander first pair of crescent chambers, x_7: pressure in the expander second pair of crescent chambers, x_8: pressure in the expander exhaust chamber; and the input variables u_1: pitch angle, u_2: supply pressure for the scroll expander. Integrating the wind turbine, driven train and PMSG sub-models, the state functions of the wind turbine system with the engaged CAES can then be described by:

$$\dot{x}_1 = x_2 \tag{26}$$

$$\begin{aligned} \dot{x}_2 = \frac{1}{J_G + J_{pass} + J_T\eta_T\varsigma_T^{\ 2} + (J_s + J_f + J_{act})\eta\varsigma^2}[&\frac{\eta_T}{2x_2}\rho_a\pi r_T^{\ 2}v_w^3 C_p(u_1) \\ &- B_{eq}\eta_T\varsigma_T^{\ 2}x_2 + \eta\varsigma\tau_s - M_f\eta\varsigma^2 x_2 - 1.5p_G(\varepsilon x_4 + L_d x_3 x_4 - L_q x_3 x_4) - F_G x_2] \end{aligned} \tag{27}$$

$$\dot{x}_3 = \frac{v_d}{L_d} - \frac{R_G}{L_d}x_3 + \frac{L_q}{L_d}p_G x_2 x_4 \tag{28}$$

$$\dot{x}_4 = \frac{v_q}{L_q} - \frac{R_G}{L_q}x_4 - \frac{L_d}{L_q}p_G x_2 x_3 - \frac{\varepsilon p_G x_2}{L_q} \tag{29}$$

$$\dot{x}_5 = -\frac{\dot{V}_c}{V_c}\gamma x_5\frac{x_2}{\varsigma} + \frac{1}{V_c}\gamma R C_d C_0 C_k A_i u_2 f(x_5/u_2)\sqrt{T_s} \tag{30}$$

$$\dot{x}_6 = -\frac{\dot{V}_s(\alpha_s,1)}{V_s(\alpha_s,1)}\gamma x_6\frac{x_2}{\varsigma} \tag{31}$$

$$\dot{x}_7 = -\frac{\dot{V}_s(\alpha_s,2)}{V_s(\alpha_s,2)}\gamma x_7 \frac{x_2}{\varsigma} \qquad \alpha_s \in [0,\ \pi] \tag{32}$$

$$\dot{x}_8 = -\frac{\dot{V}_e}{V_e}\gamma x_8 \frac{x_6}{\varsigma} + \frac{1}{V_e}\gamma R C_d C_0 C_k A_o x_8 f(p_{atm}/x_8)\sqrt{T_s} \tag{33}$$

where η_T and ς_T stands for the efficiency and ratio of the turbine shaft transmission, B_{eq} is the equivalent damping coefficient of wind turbine. If the CAES device is disengaged to the wind turbine system, we have:

$$\dot{x}_2 = \frac{1}{J_G + J_{pass} + J_T \eta_T \varsigma_T^{\ 2}}\left[\frac{\eta_T}{2x_2}\rho_a \pi r_T^{\ 2} v_w^3 C_p(u_1) - B_{eq}\eta_T \varsigma_T^{\ 2} x_2 - 1.5 p_G(\varepsilon x_4 + L_d x_3 x_4 - L_q x_3 x_4) - F_G x_2\right] \tag{34}$$

with $\dot{x}_5 = \dot{x}_6 = \dot{x}_7 = \dot{x}_8 = 0$.

3. Control strategy study for the hybrid wind turbine system

The whole hybrid system consists of several subsystems and has multi-mode operations. Thus it is necessary to develop a set of suitable decision-making rules to switch smoothly between different modes (e.g., stand-alone wind turbine and hybrid wind turbine integrated with CAES). It is also required to design dynamic control method(s) for the system performance optimization and load balance in each mode operation. The flow chart of the designed multi-mode control strategy for achieving the above objective is illustrated in Fig. 6. It can be seen that, for fully regulating the output power of the hybrid system to accurately match the load demand, the control strategy is required to cover all possible situations.

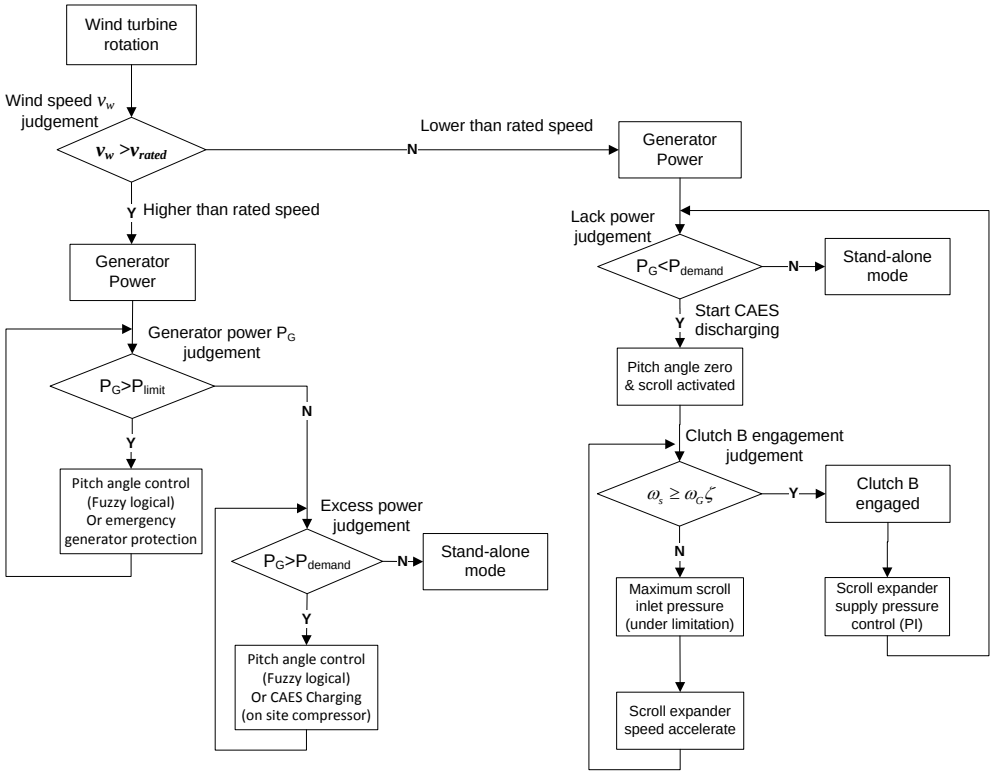

Fig. 6 Multi-mode control diagram for the proposed hybrid system

From the flow chart (Fig. 6), the main operation modes are introduced as follows: (1) while the PMSG output power is above its limitation ($P_G > P_{limit}$), the fuzzy logical control for pitch angle (or emergency generator protection) is adopted; (2) under the high wind speed situations, i.e, $v_w > v_{rated}$, if the PMSG output power is lower than its limitation but higher than the electric load demand, the fuzzy logical control for pitch angle can be maintained in the hybrid system (or surplus power can be used for CAES subsystem charging if an on-site compressor is available); (3) in the case of the insufficient PMSG output power cannot meet the electric load demand, CAES subsystem discharging mode is activated; when the scroll expander rotor speed reach a certain level, that is, $\omega_s \geq \omega_G \zeta$, Clutch B will be engaged and then the scroll expander output torque can be used to provide additional driving power to the wind turbine system; in this case, a PI controller is employed to regulate the supply pressure of the scroll expander and in turn to manage the power out of scroll expander; (4) when the PMSG output power roughly matches the electric load demand, the hybrid system will be running on the stand-alone mode, that is, Clutch B will be disengaged and the whole system will be in operation with no signal from the controller.

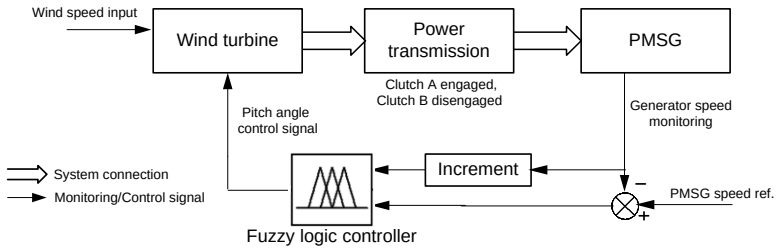

Fig. 7 Schematic of the pitch angle fuzzy logic control

Pitch angle adjustment is a common approach to regulate the aerodynamic power extracted by the wind turbine blade, which is the input power of the turbine system. A fuzzy logical controller is introduced to the designed control system for pitch angle adjustment to limit the power captured at the high wind speed situations (refer to Fig. 6). Fuzzy logic control provides a systematic way to incorporate human experience for controlling a nonlinear system, which is proved to be appropriate to such type of systems [29, 30]. Fig. 7 shows the schematic of pitch angle fuzzy logic controller implemented in the hybrid system. Choosing the speed error V_e (difference between the PMSG actual speed and the reference speed), the PMSG actual speed increment V_i and the pitch angle control value θ_p as the linguistic variables. V_e and V_i are inputs of the fuzzy logic controller, θ_p is the controller output (refer to Fig. 7). The linguistic values of V_e and θ_p are:

[NB NM NS ZO PS PM PB], which means negative big, negative middle, negative small, zero, positive small, positive middle, and positive big respectively; The linguistic values of V_i are: [N Z P], which stand for negative, zero and positive. The standard triangular membership functions have been used for both the inputs and the output of the controller. The control law is represented by a set of heuristically chosen fuzzy rules which are given in Table 1.

Table 1 Rule base for proposed fuzzy controller

θ_p		V_i		
		N	Z	P
V_e	NB	PB	PB	PM
	NM	PB	PM	PS
	NS	PM	PS	ZO
	ZO	PS	ZO	NS
	PS	ZO	NS	NM
	PM	NS	NM	NB
	PB	NM	NB	NB

Based on the triangular membership functions and the fuzzy rules, the designed fuzzy logic controller can produce a crisp and continuous nonlinear input/output map as shown in Fig. 8. This map indicates that numerous nonlinearities are designed to enhance the controller's performance to drive the system to the set point. The details related to using fuzzy logic control specific to adjust the pitch angle of wind turbines can be found in [14, 29, 30].

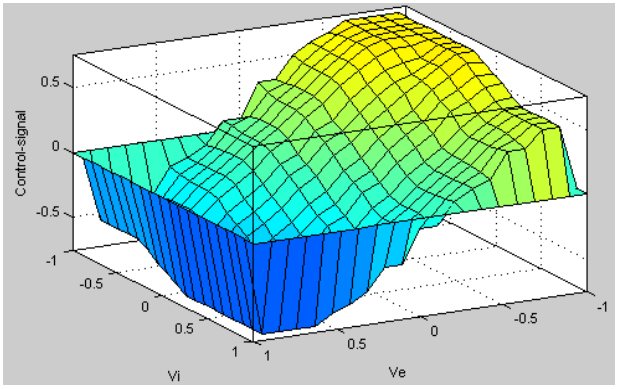

Fig. 8 Fuzzy logical controller nonlinear input & output map

During the low wind speed periods, the CAES device will work at the discharging mode to provide additional driving power. For controlling the input power from the CAES device to the wind turbine system, it is necessary to manage how much compressed air flows into the scroll expander at every moment. Considering the limited central chamber volume of the scroll expander, the supply air pressure control by a digital

proportional pressure regulator is more suitable to achieve this purpose, compared to the traditional pneumatic valve displacement control. A PI control method on the pressure regulator is chosen because of its simplicity. Fig. 9 shows the schematic of the scroll expander supply pressure PI control. The controller input is the PMSG speed tracking error $e(t)$, i.e., $e(t) = \omega_{ref} - \omega_G$, where ω_{ref} is the PMSG reference speed. The control law can be represented as:

$$U(t) = K_P e(t) + K_I \int e(t) + C_{initial} \tag{35}$$

where K_P and K_I are the proportional and integral control gains, $C_{initial}$ represents the initial controller reference value. In addition, during the low wind speed periods, it is common to set the pitch angle θ equals to zero for achieving the best turbine efficiency C_p (refer to Subsection 2.1 and Fig. 9).

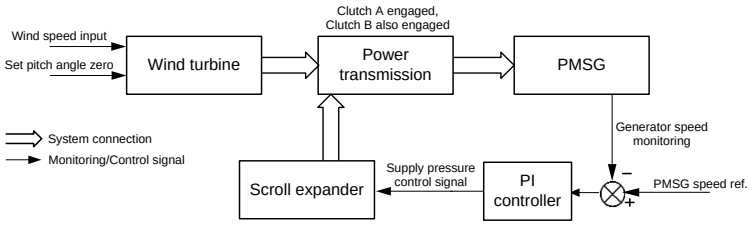

Fig. 9 Schematic of the scroll expander supply pressure PI control

4. Simulation study for the hybrid system

The overall state space model of the hybrid wind turbine with the CAES system and its corresponding multi-mode control strategy are implemented in Matlab/Simulink environment for simulation study. The parameters for the simulation study of the whole hybrid system are listed in Table 2. Most parameters related to the scroll expander, the drive train and the PMSG are obtained from the associated data sheets or measurement of the machines which are used for building the experimental test rig in the laboratory. However, due to the complicated structure of the hybrid system, sometimes it is difficult to obtain the precise values for all parameters. These unknown parameters for models can be identified using intelligent computational algorithms together with the experimental data [31].

Table 2 Parameters of the hybrid wind turbine system

Symbol	Description	Value
J_T	inertia of turbine blades	4.9 kg × m^2
ρ_a	Air density	1.25 kg/m^3
r_T	Blade radius	1.75 m
ς_T	Speed ratio of turbine shaft transmission	5
η_T	Efficiency of turbine shaft transmission	0.95
η	Transmission efficiency of the belt	0.95
r_s	Orbit radius of the scroll	5.40×10^{-3} m
z	Depth of the scroll chambers	3.33×10^{-2} m

V_{total}	Total control volume of the scroll	2.50×10^{-4} m^3
p_G	The number of pole pairs	6
R_G	Resistance of the PMSG stator windings	1.31 Ohm
L_d	Inductance on d axis	2.075 mH
L_q	Inductance on q axis	2.075 mH
λ	Flux amplitude induced by permanent magnets	0.171Wb

The simulation considers the scenario when the input mean wind speed steps down within a 40 seconds' time series observation window, as shown in Fig. 10. A white noise source with a shaping filter is chosen to generate the input wind speed profile, and its feasibility had been studied in [32-34]. From Fig. 10, it can be seen that the mean wind speed drops from around 10 m/s to 8 m/s at the moment of the 20th second. Thus the simulated data can represent the wind speed variation in a certain period.

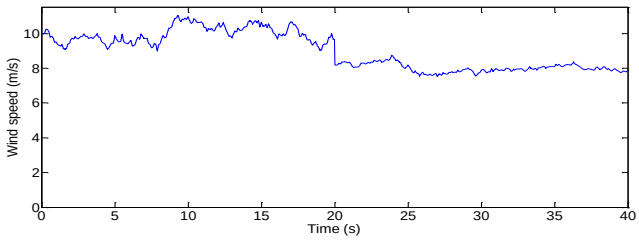

Fig. 10 Simulated wind speed profile

Introducing the simulated wind speed profile given in Fig. 10 to the hybrid system input, Fig. 11 shows the comparisons of dynamic responses of the multi-mode controlled hybrid system and the stand-alone wind turbine system without any controller implementation, which include the variation history comparisons of the PMSG speeds and the wind turbine main shaft torques. To a given electric resistance load, the PMSG reference speed is set to 190 rad/s. From Fig. 11, it is clearly seen that, during low wind speed periods, the PMSG can obtain additional driving torque from small-scale CAES integration, thus the simulated hybrid system with the PI controller connected can compensate the required electric power efficiently; meanwhile, during high wind speed periods, the designed system with the fuzzy logic controller activated can track the reference speed very well, which may reveal only few extra load and tiny inertia added by the mechanical power transmission. Furthermore, it looks that the performance of PI control to the scroll expander supply pressure is not as good as that of the pitch angle fuzzy logic control. This could be resulted from the high nonlinearity characteristics of the compressed air.

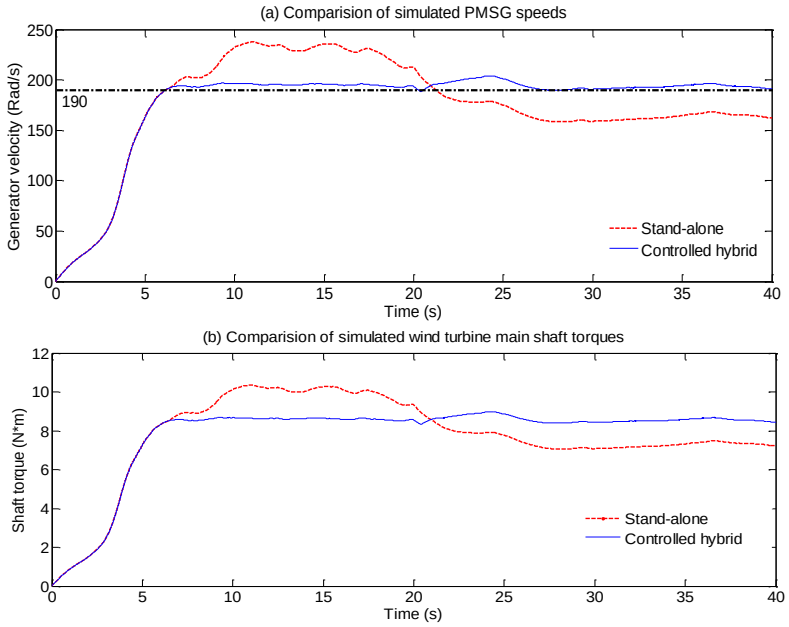

Fig. 11 Comparison of dynamic responses of the hybrid system with designed controllers connected and the stand-alone wind turbine without any control

Correspondingly, Fig. 12 shows the simulation results of the dynamic responses of the controlled variables in the hybrid system when the input wind speed profile is given as Fig. 10. In the designed system, the pitch angle and the supply pressure of the scroll expander are the controlled variables. From Fig. 12 (a), it can be observed that, under the conditions of high wind speed, the pitch angle varies within the range from 0 to 11 degrees. This is because the pitch angle is adjusted by fuzzy logic control to maintain a relatively steady wind power output for the PMSG speed getting close to the required reference (190 rad/s). At low speed situations, the pitch angle is set to 0 degree for maximizing the capability of wind turbine blades to extract the wind energy. In Fig. 12 (b), the variation history of the supply pressure of scroll expander is presented. The expander is activated at 20 seconds from the time at which the wind turbine are in operation. Once Clutch B is engaged, its supply pressure is always managed by the designed PI controller. From the simulation study, the scroll expander can speed up very quickly after its activation, mainly due to the expander small inertia.

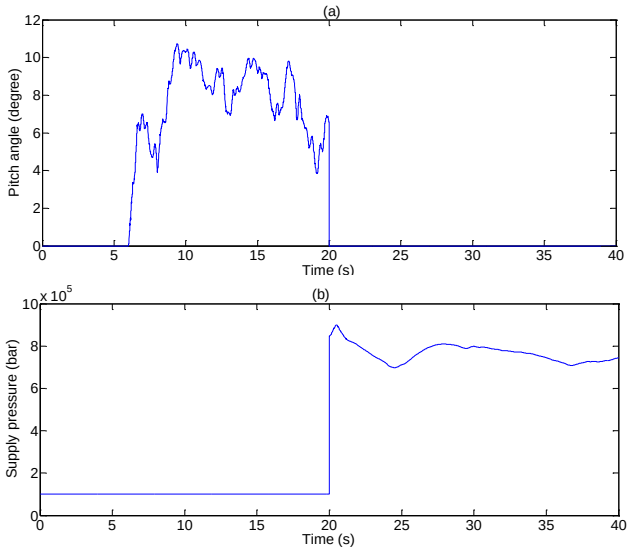

Fig. 12 Dynamic responses of the controlled variables in the hybrid system

5. Experimental Tests

An experimental test rig corresponding to the designed hybrid system is built in the authors' research laboratory at the University of Warwick, as shown in Fig. 13. The block diagram of this prototype test rig is illustrated in Fig. 14. Due to the limitation of indoor laboratory work, the test rig uses a "Wind Turbine Simulator (WTS)" to replace the practical wind turbine blade, which consists of dual DC motors, their power supplies and some auxiliaries (Fig. 14). The function of this simulator is to mimic the real fluctuant turbine blade torque and wind power scenario. The reasonability of WTS had been proven in some literatures, e.g., [32, 33].

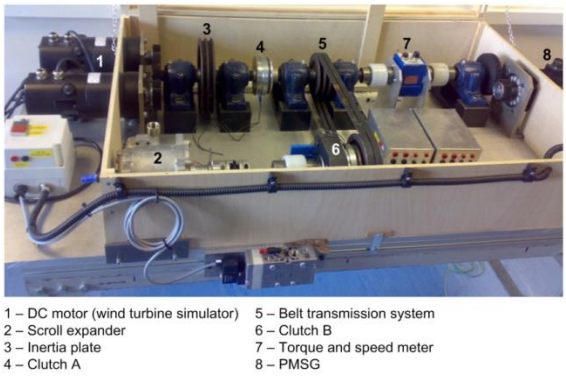

Fig. 13 The experimental test rig of the wind turbine system integrated with small-scale CAES

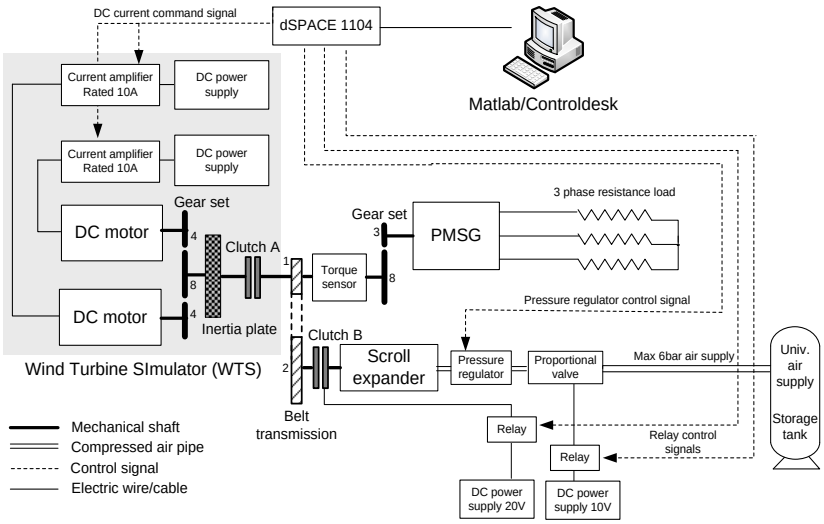

Fig. 14 Block diagram of the test rig of the wind turbine system integrated with small-scale CAES

Based on Fig. 14, the main test system components are listed in Table 3. The test rig consists of duel DC motors, a PMSG and its 3-phase resistance load, a scroll expander, a compressed air storage tank, a belt transmission subsystem, two clutch mechanisms, two gear sets, a pneumatic valve, a digital pressure regulator, DC power supplies, sensors and meters for electrics and pneumatics, etc. The employed scroll expander is modified from a scroll compressor (Table 3). In addition, two gears sets (Fig. 14) as speed match devices are applied to ensure that each facility can work around at its rated condition. The speed ratios to the gear sets are determined by the rated speeds of these facilities.

Table 3 Machines for the experimental test system

Name	Serial number/description	Manufacturer
DC motor	SN:M4-2952X-2100t-000	Callan Tech.
PMSG	SN:SGMSS-20A	Yaskawa Elec.
Scroll expander	Modified from compressor TRSA090	Sanden
Air tank	Max 6 bar from univ. storage tank	BOC UK
Controller	Model: RTI1104	dSPACE
Clutch A	SN:CS-10-31G, 24V	Mikipulley
Clutch B	101-10-15G, 24V	Mikipulley
DC power supply	90Vdc, 0-10Adc, for DC motor	TRM Elec.
DC amplifier	SN:10/100, 24-100Vdc, 0-10Adc	TRM Elec.
Voltage transducer	SN:LV 25-P, ±10V	LEM
Current transducer	SN:LTSR 15-NP, ±15A	LEM
Pressure sensor	SN:SDE1-D10-G2-W18-L-PU-M8	FESTO
Flow meter	SN:MS6 SFE-F5-P2U-M12	FESTO
Pressure regulator	SN:VPPM-6L-L-1-G18-0L10H-V1N	FESTO
Pneumatic valve	SN:MYPE-5-1/4-010-B, 0-10 bar	FESTO
Torque sensor	SN:RWT 310, 0-2000 RPM	Sensor Tech.
Temperature sensor	K-type thermocouple	RS UK

A dSPACE real-time controller (Model: RTI1104) is chosen for collecting the experimental data from electric and pneumatic sensors. The experimental data is monitored and collected in dSPACE Controldesk/Matlab environment. This real-time controller is also used for controlling the whole hybrid system operations, which include activating the scroll expander, engaging Clutch B (Clutch A is always engaged as described in Section 2), implementing PI control to the pressure regulator and managing the WTS torque output to the hybrid system (refer to Fig. 14).

Fig. 15 illustrates the block diagram of the WTS in the hybrid system test rig. The WTS can be considered as a variant of Rapid Control Prototyping (RCP) – using simple PID control to command duel DC motors for mimicking the real wind turbine behaviours. Similarly to the simulation study, a white noise source with a shaping filter is used to generate the wind speed profile ([32-34]). A typical torque-current closed loop PID control is implemented on the DC motors as shown in Fig. 15.

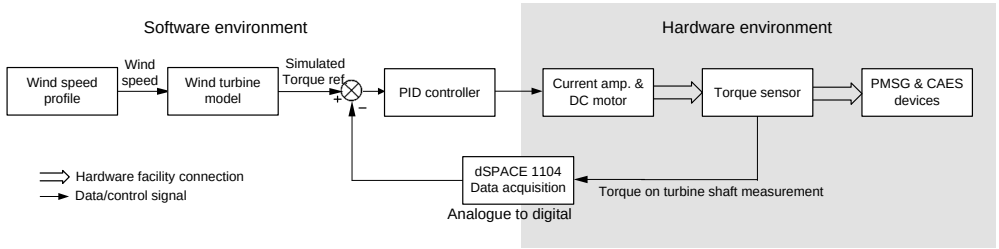

Fig. 15 Block diagram of the WTS in the hybrid system test rig

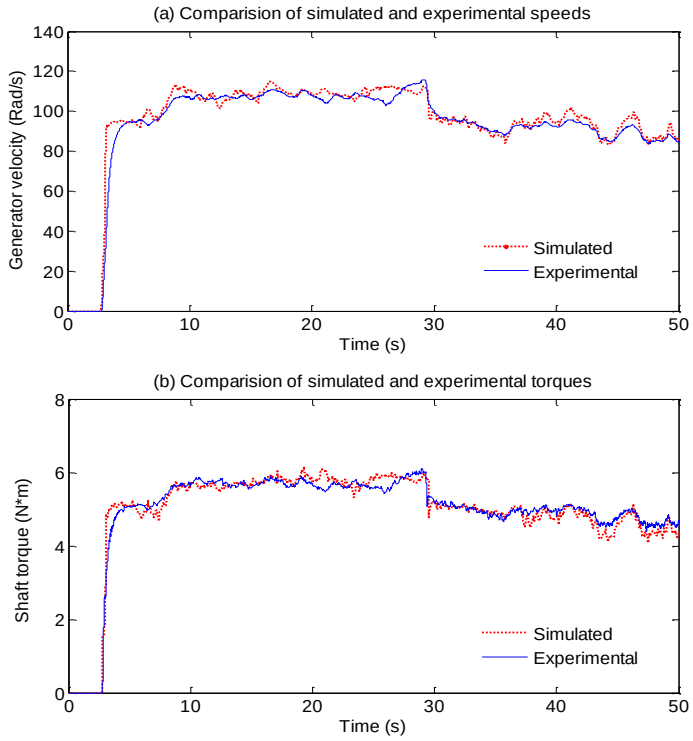

Fig. 16 Comparisons of the test results and the simulated data for the WTS

The comparisons of the experimental test results and the simulated data for the WTS are given in Fig. 16, including the wind turbine shaft speeds and torques respectively. It can be seen that the experimental dynamic performance of the WTS torque can track well to that of the simulated torque reference. From the experimental tests, it is proven that the WTS can meet the laboratorial requirements to mimic the practical scenarios of wind power generation systems.

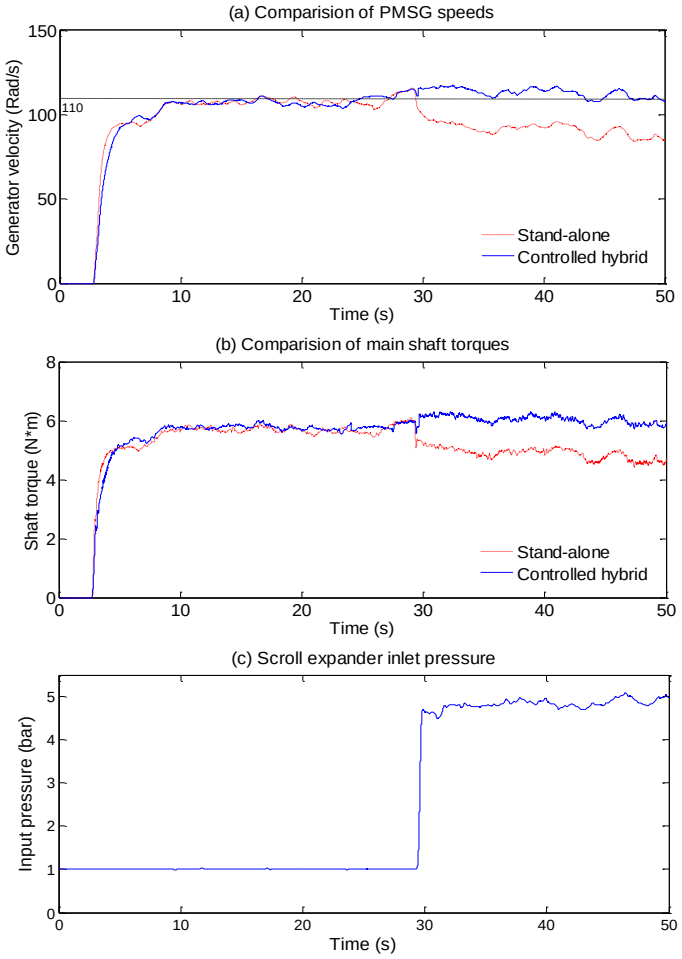

Fig. 17 Experimental test results of the stand-alone wind turbine and the controlled hybrid system

Due to the laboratory limitations and the university safety regulations, the experimental test to the hybrid system with the control strategy implemented mainly focuses on the study of system operation under low wind speed situations. It is for observing the test rig dynamic responses at the moment of Clutch B engagement and the controller performance to the CAES subsystem for compensation work. Fig. 17 shows the comparisons of the experimental test results of the hybrid system under the wind turbine stand-alone mode and the wind turbine integrated CAES with controller connected mode. The speed reference is set to 110 rad/s. It can be seen that, with the CAES integration and the scroll expander supply pressure control, the designed experimental test system can maintain relatively steady outputs and to meet the speed reference under the low

wind speed conditions. The CAES system can contribute controllable mechanical power to the hybrid wind turbine system for generating required electricity. Thus the experiment results shown in Fig. 17 verify that the idea proposed in this paper is feasible and the corresponding prototype can work properly.

6. Efficiency analysis

To the situation of controlled hybrid system operation, the power transmission and conversion from a small-scale CAES to the wind turbine system is schematically illustrated in Fig 18. The scroll expander converts the energy extracted from the stored compressed air into the useful mechanical energy which is in turn transferred to the wind turbine main shaft through the belt transmission system. For such process, energy losses are inevitable, such as the scroll expander operation loss due to friction, vibration, air leakage, lubricant viscosity, etc.

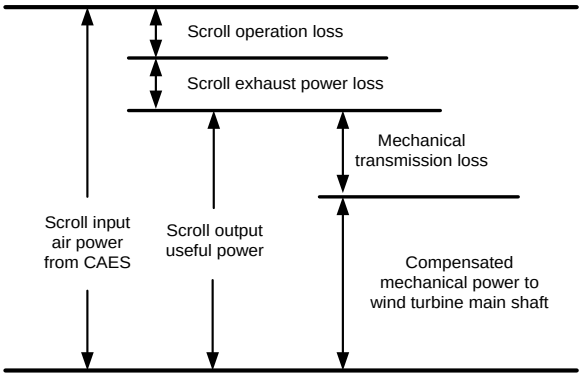

Fig.18 Power transmission and conversion from the small-scale CAES to the wind turbine system

The power efficiency of the engaged CAES system in this paper is defined as,

$$\eta_{eff} = \frac{Increased\ \ mechanical\ \ power\ \ resulted\ \ from\ CAES\ compensation}{Input\ compressed\ air\ power\ \ from\ CAES} \tag{36}$$

This power efficiency reveals the performances of the designed small-scale CAES facility and the mechanical power transmission. In addition, the increased mechanical power resulted from CAES compensation is considered as the difference of the hybrid system main shaft powers between the stand-alone mode and hybrid mode under the same driving conditions.

From the above description, it is necessary to quantitatively analysis how much air power/energy carried by compressed air enters into the scroll expander. One simplified approach is adopted for calculating the input air power referred to STP (Standard Temperature and Pressure, 0 ^{o}C at 1 bar), which is ([35, 36]):

$$\dot{Q}_{in} = \dot{m}_{in} RT_{atm}[\ln \frac{p_{in}}{p_{atm}} + \frac{k}{k-1}(\frac{T_{in}}{T_{atm}} - 1 - \ln \frac{T_{in}}{T_{atm}})] \quad (37)$$

where $\dot{Q}_{in}$ is the input air power to the scroll expander, $\dot{m}_{in}$ is the input air mass flow rate, T is temperature, p is pressure, k is the specific heat ratio, subscript atm means atmospheric state and in is inlet thermodynamic state. When the environment shifts 100 K from the atmospheric temperature, the temperature variation to the change of air power is limited ([35, 36]). Thus it can assume $T_{in} = T_{atm}$ and then substituting this into Eq. (37), the air power can be calculated by,

$$\dot{Q}_{in} = \dot{m}_{in} RT_{atm} \ln \frac{p_{in}}{p_{atm}} = p_{atm} w_{in} \ln \frac{p_{in}}{p_{atm}} \quad (38)$$

where w_{in} is the input volumetric air flow rate.

Building upon the available sensors in the laboratory for data acquisition, three groups of experimental tests of the hybrid system are implemented to analyse the power efficiency. The experimental results are given in Table 4. The tests are conducted under the condition of maintaining the Wind Turbine Simulator (WTS) power output at three different levels, which result in three measured power levels of shaft power under the wind turbine stand-alone mode, which are 640, 510 and 390 watts respectively (Table 4). Also, in each group of the tests, the hybrid system is operated at the different inlet air pressures to the scroll expander for the power efficiency comparison.

Table 4 Power efficiency analysis based on the experimental data

Inlet pressure (bar)	Inlet flow rate (L/min)	Scroll inlet temperature (^oC)	Scroll outlet temperature (^oC)	Stand-alone power (W)	Hybrid power (W)	Power Efficiency (%)
5.76	335	24.5	17	640	980	34.76%
4.90	255	24.5	17.5	640	950	45.87%
3.95	230	24.5	18	640	900	49.34%
5.75	340	24.5	17.2	510	925	41.84%
4.88	250	24.5	17.6	510	875	55.27%
3.90	220	24.5	18.1	510	780	54.07%
5.73	320	24.5	17.2	390	800	44.01%
4.90	245	24.5	17.7	390	690	46.20%
3.90	205	24.5	18.1	390	610	47.28%

From the experimental results, it can be found that, in each group of the tests, the variations of the power efficiency are relevant to the scroll expander inlet air pressure, which indicates that the air pressure and mass

flow rate should be well managed and controlled to achieve higher efficiency. According to this, under a given working condition, it may suggest using lower inlet pressures of compressed air for obtaining higher power efficiencies. From Table 4, the maximum power efficiency is around 55%. The main reason for this moderate efficiency is that CAES and pneumatic drives have relatively low efficiencies in general. From the reported figures, in most cases, around 20-30% energy efficiency can be achieved for pneumatic actuator (drive) systems; 45-54% cycle efficiency has been reported for the existing commercialized large-scale CAES plants [9, 22, 35, 36]. Although the scroll expander has relatively higher energy conversion ability compared to traditional pneumatic actuators ([23, 24]), the efficiency related to CAES and its components is still a key issue which needs further research and development. Also, considering the moderate efficiency of CAES and pneumatic drives, the power efficiency analysis indicates that the designed mechanical power transmission for the hybrid system can deliver an acceptable performance.

7. Conclusion

In this paper, a new concept of hybrid system is proposed, which consists of a kW-level wind turbine integrated with a small-scale CAES unit. To avoid mechanical force coupling between the driving torques from wind power and the air expander, a mechanical transmission mechanism is developed to smoothly integrate the two torque sources. The complete dynamic mathematical model of the hybrid system is developed and implemented in Matlab/Simulink simulation environment for comprehensive simulation study of system dynamic behaviours. An appropriate control strategy is developed for the system to smooth the transient fluctuations and compensate the energy gap of wind power generation. A prototype system is built and installed in the research lab for verifying the design idea. From both the simulation and test results, the hybrid wind turbine system can generate the reliable steady power output with the compensation power from CAES. It can be concluded that the proposed hybrid system of wind turbines and CAES is feasible with a great potential for future industrial applications.

The energy conversion efficiency from the compressed air energy to the electrical power output has been investigated with various operation conditions. The system test results indicated that the efficiency can be up to 55% under a well-controlled operation condition, which is higher than the typical pneumatic actuator efficiency. The findings have provided essential evidences and information for the next stage of research which will lead to improved efficiency and reliability.

Acknowledgement:

The authors would like to thank Advantage West Midlands and the European Regional Development Fund, funders of the Science City Research Alliance Energy Efficiency Project – a collaboration between the Universities of Birmingham and Warwick and UK Engineering and Physical Sciences Research Council (EPSRC, EP/K002228/1) for the funding support.

References

[1] Global Wind Energy Council. Global statistics n.d. [Online]. Available at: http://www.gwec.net/global-figures/graphs/. [Accessed: 16- Feb - 2014].

[2] Gul T, Stenzel T. Intermittency of wind: the wider picture. Int J Glob Energy Issues 2006;25:163–86.

[3] Roy S. Impact of short duration wind variations on output of a pitch angle controlled turbine. Sustain Energy, IEEE Trans 2012;3:566–75.

[4] Houwing M, Papaefthymiou G, Heijnen PW, Ilic MD. Balancing wind power with virtual power plants of micro-CHPs. PowerTech, 2009 IEEE Bucharest, IEEE; 2009, p. 1–7.

[5] Chen Z, Guerrero JM, Blaabjerg F. A review of the state of the art of power electronics for wind turbines. Power Electron IEEE Trans 2009;24:1859–75.

[6] Díaz-González F, Sumper A, Gomis-Bellmunt O, Villafáfila-Robles R. A review of energy storage technologies for wind power applications. Renew Sustain Energy Rev 2012;16:2154–71.

[7] Le HT, Santoso S. Operating compressed-air energy storage as dynamic reactive compensator for stabilising wind farms under grid fault conditions. IET Renew Power Gener 2013;7:717–26.

[8] Cavallo A. Controllable and affordable utility-scale electricity from intermittent wind resources and compressed air energy storage (CAES). Energy 2007;32:120–7.

[9] Succar S, Williams RH. Compressed Air Energy Storage: Theory, Resources,And Applications For Wind Power. 2008.

[10] Sun H, Luo X, Wang J. Management and control strategy study for a new hybrid wind turbine system. IEEE Conf. Decis. Control Eur. Control Conf., IEEE; 2011, p. 3671–6.

[11] RWE power. ADELE – Adiabatic compressed-air energy storage (CAES) for electricity supply n.d. [Online]. Available at: http://www.rwe.com/web/cms/en/365478/rwe/innovation/projects-technologies/energy-storage/project-adele/. [Accessed: 07-Nov-2012].

525 [12] Finkenrath M, Pazzi S, D'ercole M, Marquardt R, Moser P, Klafki MZS. Status and Technical
526 Challenges of Advanced Compressed Air Energy Storage (CAES) Technology. 2009 Int. Work. Environ.
527 Altern. Energy, Monachium, 2009.
528 [13] Yang Y, Emadi A. Integrated electro-mechanical transmission systems in hybrid electric vehicles. IEEE;
529 2011.
530 [14] Madlener R, Latz J. Economics of centralized and decentralized compressed air energy storage for
531 enhanced grid integration of wind power. Appl Energy 2013;101:299–309.
532 [15] Marano V, Rizzo G, Tiano FA. Application of dynamic programming to the optimal management of a
533 hybrid power plant with wind turbines, photovoltaic panels and compressed air energy storage. Appl
534 Energy 2012;97:849–59.
535 [16] Succar S, Denkenberger DC, Williams RH. Optimization of specific rating for wind turbine arrays
536 coupled to compressed air energy storage. Appl Energy 2012;96:222–34.
537 [17] Li Y, Wang X, Li D, Ding Y. A trigeneration system based on compressed air and thermal energy storage.
538 Appl Energy 2012;99:316–23.
539 [18] Heier S. Grid integration of wind energy conversion systems. Wiley; 1998.
540 [19] Sun H, Wang J, Guo S, Luo X. Study on energy storage hybrid wind power generation systems. Proc.
541 World Congr. Eng., 2010, p. 833–8.
542 [20] Mathworks. Matlab R2012a Documentation-SimPowerSystems n.d. [Online]. Available at:
543 http://www.mathworks.co.uk/help/physmod/sps/powersys/ref/windturbine.html/. [Accessed: 31-Oct-
544 2013].
545 [21] Mihet-Popa L, Blaabjerg F, Boldea I. Wind turbine generator modeling and simulation where rotational
546 speed is the controlled variable. Ind Appl IEEE Trans 2004;40:3–10.
547 [22] Wang J, Yang L, Luo X, Mangan S, Derby JW. Mathematical Modeling Study of Scroll Air Motors and
548 Energy Efficiency Analysis—Part I. Mechatronics, IEEE/ASME Trans 2011;16:112–21.
549 [23] Yanagisawa T, Fukuta M, Ogi Y, Hikichi T. C591/027/2001 Performance of an oil-free scroll-type air
550 expander. IMechE Conf. Trans., vol. 7, Professional Engineering Publishing; 1998; 2001, p. 167–76.
551 [24] Wang J, Luo X, Yang L, Shpanin LM, Jia N, Mangan S, et al. Mathematical Modeling Study of Scroll
552 Air Motors and Energy Efficiency Analysis-Part II. Mechatronics, IEEE/ASME Trans 2011;16:122–32.
553 [25] Yang L, Wang J, Lu N, Mangan S, Derby JW. Energy Efficiency Analysis of a Scroll-type Air Motor
554 Based on a Simplified Mathematical Model. Proc. World Congr. Eng. 2007, London: 2007.

555 [26] Dehkordi AB, Gole AM, Maguire TL. Permanent magnet synchronous machine model for real-time
556 simulation. Int. Conf. power Syst. transients, 2005.
557 [27] Fitzgerald AE, Kingsley C, Umans S. Electric Machinery, 6/e. Ed; 1983.
558 [28] Pillay P, Krishnan R. Modeling, simulation, and analysis of permanent-magnet motor drives. I. The
559 permanent-magnet synchronous motor drive. vol. 25. 1989.
560 [29] Chen WL, Hsu YY. Unified voltage and pitch angle controller for wind-driven induction generator
561 system. Aerosp Electron Syst IEEE Trans 2008;44:913–26.
562 [30] Chowdhury MA, Hosseinzadeh N, Shen W. Fuzzy logic systems for pitch angle controller for smoothing
563 wind power fluctuations during below rated wind incidents. PowerTech, 2011 IEEE Trondheim, IEEE;
564 2011, p. 1–7.
565 [31] Wei J-L, Wang J, Wu QH. Development of a Multisegment Coal Mill Model Using an Evolutionary
566 Computation Technique. Energy Conversion, IEEE Trans 2007;22:718–27.
567 [32] Nichita C, Luca D, Dakyo B, Ceanga E. Large band simulation of the wind speed for real time wind
568 turbine simulators. Ieee Trans Energy Convers 2002;17:523–9.
569 [33] Li W, Xu D, Zhang W, Ma H. Research on wind turbine emulation based on DC motor. Ind. Electron.
570 Appl. 2007. ICIEA 2007. 2nd IEEE Conf., IEEE; 2007, p. 2589–93.
571 [34] Welfonder E, Neifer R, Spanner M. Development and experimental identification of dynamic models for
572 wind turbines. Control Eng Pract 1997;5:63–73.
573 [35] Cai M, Kagawa T. Energy consumption assessment of pneumatic actuating systems including compressor.
574 Int. Conf. Compressors their Syst., London, UK: 2001, p. 381–90.
575 [36] Cai M, Kawashima K, Kagawa T. Power assessment of flowing compressed air. J Fluids Eng
576 2006;128:402–5.